

# Observation of improved and degraded confinement with driven flow on the LAPD

D.A. Schaffner,<sup>1</sup> T.A Carter,<sup>1</sup> G.D. Rossi,<sup>2</sup> D.S. Guice,<sup>1</sup> J. Maggs,<sup>1</sup> S. Vincena,<sup>1</sup> and B. Friedman<sup>1</sup>

<sup>1</sup>*Department of Physics and Astronomy,  
University of California, Los Angeles.*

<sup>2</sup>*Department of Physics, University of Texas, Austin*

(Dated: May 10, 2012)

## Abstract

Continuous control over azimuthal flow and shear in the edge of the Large Plasma Device (LAPD) has been achieved using a biasable limiter which has allowed a careful study of the effect of flow shear on pressure-gradient-driven turbulence and transport in LAPD. LAPD rotates spontaneously in the ion diamagnetic direction (IDD); positive limiter bias first reduces, then minimizes (producing a near-zero shear state), and finally reverses the flow into the electron diamagnetic direction (EDD). Degradation of particle confinement is observed in the minimum shearing state and reduction in turbulent particle flux is observed with increasing shearing in both flow directions. Near-complete suppression of turbulent particle flux is observed for shearing rates comparable to the turbulent autocorrelation rate measured in the minimum shear state. Turbulent flux suppression is dominated by amplitude reduction in low-frequency ( $> 10\text{kHz}$ ) density fluctuations and a reduction in the radial correlation length. An increase in fluctuations for the highest shearing states is observed with the emergence of a coherent mode which does not lead to net particle transport. The variations of density fluctuation and radial correlation length are fit well with power-laws and compare favorably to simple models of shear suppression of transport.

While flow shear does provide a source of free energy for instability and turbulence [], it can lead to stabilization of pressure-gradient-driven instabilities and a reduction of turbulent transport in magnetized plasmas [1, 2]. The transport barrier in the high-confinement mode, or H-mode, of tokamak operation [3] is attributed to the spontaneous development of an edge flow layer in which strong shearing suppresses transport [1? , 2]. The direct connection between the H-mode edge flow layer and improved confinement was first established in experiments on the Continuous Current Tokamak (CCT) in which transport barriers were generated by directly driving edge flow using torque due to radial currents driven by biased electrodes [4, 5]. Biasing has been used to produce improved confinement in a number of subsequent experiments including toroidal devices [6–11] and linear magnetized plasmas [12–14]. Turbulence can self-regulate through the generation of flows and flow shear (zonal flows); this effect is often invoked to explain saturation of drift turbulence and as a possible explanation for spontaneous confinement transitions in fusion devices [2, 15]. Direct evidence for turbulent-Reynolds-stress-driven flow has been reported in a cylindrical magnetized plasma device [? ].

While ample evidence for transport reduction in the presence of sheared flow exists [16?] and significant effort and progress has been made in developing a theoretical understanding the interaction between sheared flow and turbulence, there are still a number of open questions that can be answered by experiment. In particular, the exact mechanism behind turbulence modification and transport suppression occur in the presence of shear is still subject to debate: theories present a number of mechanisms including radial decorrelation [17], nonlinear reduction of turbulent amplitude [? ], and modification of turbulent cross-phase [18]. Evidence for all of these mechanisms exists in experimental data [16], but a comprehensive experimental dataset establishing in detail the parameter regimes where each mechanism is important has not been acquired. In part, this is due to the fact that most datasets on flow-turbulence interaction come from studies of spontaneously generated flow or in cases where precise external control over flow and flow shear is not possible. A number of basic plasma experiments have utilized biasing techniques to drive flow and flow shear to study flow driven instabilities (e.g. [19? ]), however experiments have not been successfully done in which precise external control over flow and flow shear has been achieved in the presence of drift-wave turbulence to systematically study the changes in turbulence characteristics and transport.

In this letter, we report on the first experiments in which external control of flow is used to document the response of turbulence and transport to a continuous variation of flow shear, including a zero shear state and a reversal of the flow direction. Shearing rates ( $\omega_s = \partial V_\theta / \partial r$ ) from zero to up to five times the turbulent autocorrelation rate measured at zero flow shear ( $\Delta\omega_d$ ) are achieved. Turbulent particle flux is reduced with increasing shearing rate, regardless of the direction of the flow or sign of the flow shear, with significant reduction occurring for  $\omega_s \sim \Delta\omega_d$ . The observed reduction in particle flux is dominated by decreases in low-frequency ( $f < 10\text{kHz}$ ) density fluctuation amplitude and a reduction of the radial correlation length is also observed. For low frequency fluctuations, the crossphase between density and azimuthal electric field fluctuations remain near zero for all shearing rates. With higher shear ( $\omega_s > \Delta\omega_d$ ) we observe the emergence of a coherent mode localized spatially in the region of strong flow. Fluctuations from this mode appear to increase density fluctuations above 10kHz, but do not appear to contribute to particle flux.

The Large Plasma Device [20] (LAPD) is a 17m long,  $\sim 60\text{cm}$  diameter cylindrical plasma produced by a barium-oxide coated nickel cathode. In the experiments reported here, a plasma of density  $\sim 2 \times 10^{12} \text{ cm}^{-3}$  and peak temperature of  $\sim 8\text{eV}$  is produced in a uniform magnetic field of 1000G. Measurements of electron density, electron temperature, and potential (both plasma potential and floating potential) are made using Langmuir probes. Measurements of ion saturation current ( $I_{\text{sat}} \propto n_e \sqrt{T_e}$ ) and floating potential ( $V_f$ ) are taken with a 9-tip Langmuir probe (flush-mount tantalum tips) probe while temperature and plasma potential is determined using a swept Langmuir probe. Turbulent particle flux  $\Gamma = \langle \tilde{n}_e \tilde{E}_\theta \rangle$  is determined through correlating  $I_{\text{sat}}$  fluctuations from one tip of this probe with azimuthal electric field fluctuations ( $E_\theta$ ) derived from floating potential fluctuations on two azimuthally separated tips. Azimuthal  $E \times B$  flow is computed using the swept-probe-derived plasma potential. Flows derived using this technique during these experiments compare very well to measurements using Mach probes [13] and flows derived from time-delay estimation (TDE) of the velocity of turbulent structures [].

Biassing experiments have been previously conducted on LAPD in which edge profile steepening and a reduction in turbulent flux was observed [13, 14]. In these experiments, edge flow was driven through biassing the vacuum chamber wall with respect to the plasma source cathode. Transport reduction occurred only for biases above a threshold value. Below the threshold, azimuthal flow was localized near the biased wall and no flow or flow shear

was driven in the region where drift wave turbulence exists. Above the threshold, the flow was able to penetrate radially inward and strong flow and flow shear, with shearing rate far above the low-flow turbulent autocorrelation rate, was driven in the region of strong density gradient. Recent experiments were successful in more continuous control of potential and cross-field flow in the shadow of a biased obstacle inserted into the LAPD core plasma [21]. Both confinement improvement and degradation (formation of strong density depletions) were observed with the density profile created by the obstacle in this case.

Building on the success of biasing obstacles to control flow, an annular aluminum limiter was installed in LAPD. The provides a parallel boundary condition for the edge plasma and is biased relative to the cathode of the plasma source to control plasma potential and cross-field flow. The limiter is an iris-like design with four movable plates and is located 2.5m from the cathode. In these experiments, the limiter plates were adjusted to provide a provide a 52cm diameter aperture; downstream of the limiter, plasma on field lines with radial location  $r > 26\text{cm}$  sees the limiter as a conducting end boundary condition and plasma on field lines for  $r < 26\text{cm}$  sees the anode/cathode of the source region as a parallel boundary condition. A capacitor back connected to a transistor switch supplies a bias voltage pulse to the limiter. The bias pulse lasted 5ms during the flattop of the  $\sim 15\text{ms}$  plasma discharge. The limiter was biased from  $\sim 10\text{V}$  below the anode potential to  $50\text{V}$  above the anode voltage. Typically plasma potential in the core LAPD plasma (plasma on field lines that connect to the source region) is very close to the anode voltage and the cathode sits near ground (vacuum chamber wall). The anode potential is above the cathode potential by the discharge voltage, which was  $40\text{V}$  during these experiments.

Spontaneous rotation of the LAPD is observed when the limiters are unbiased (here the limiters are observed to float to a potential  $\sim 10\text{V}$  below the anode). In this state, an edge flow (peaked just outside the limiter edge) is observed in the ion diamagnetic direction (IDD), as shown in Fig. 1(a). Biasing the limiter positively with respect to the cathode tends to drive flow in the electron diamagnetic direction (EDD). As the limiter bias is increased, the flow in the IDD is first reduced, then reaching near-zero flow and flow-shear states, and is ultimately reversed with strong EDD flow.

Measurements of profiles of density ( $I_{\text{sat}}$ ) and particle flux were made for each bias flow state. Values are averaged over a range from 27 to 31cm, a region where average flow and flow shear scale nearly linearly with limiter bias, as shown in Fig. 1(b).

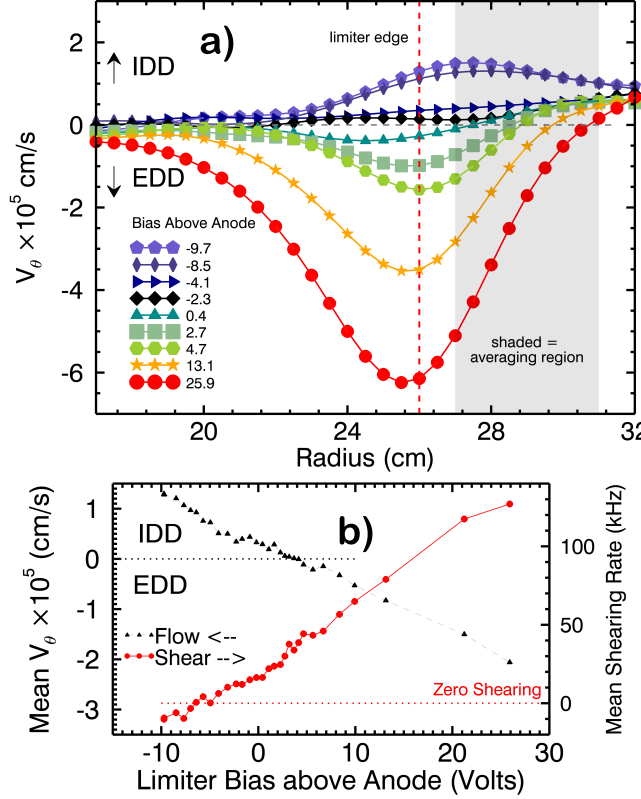


FIG. 1: (a) Velocity profiles using plasma potential from swept measurements. (b) Nearly linear scaling of flow (black) and shearing (red) versus limiter bias. Note that the zero in mean absolute shear does not occur at zero average flow.

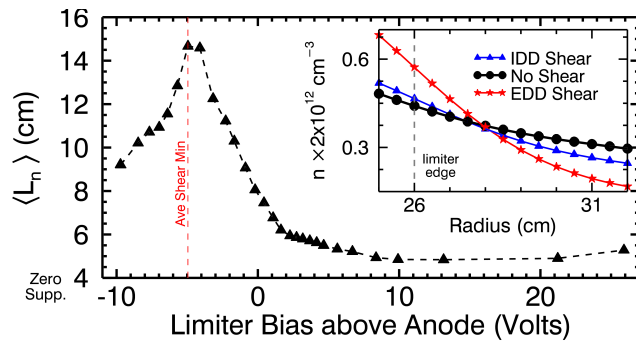


FIG. 2: Density gradient length scale versus limiter bias. Inset shows density profile relaxing then steepening again with bias.

Fig. 2 shows the variation in the spatially-averaged density gradient length scale,  $L_n = |\nabla \ln n|^{-1}$  with increasing limiter bias. As the limiter bias is increased, reducing the IDD flow, an increase in the gradient scale length is observed, indicating a degradation of radial particle confinement which peaks when the averaged shearing rate is near zero. As the bias is increased further, reversing the flow and again increasing the shearing rate, the density gradient gradually steepens and the scale length is lowered, indicating improved particle confinement.

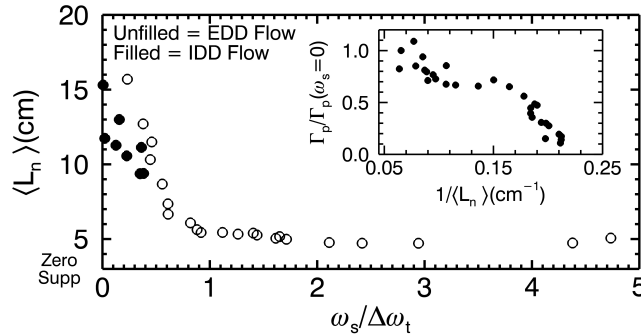


FIG. 3: Gradient scale length versus shearing rate. Inset shows correlation of gradient scale length and turbulent particle flux. Note how this data is inconsistent with a Fick's Law like diffusion, which would be identified by a linearly increasing flux with gradient.

The observed variation of  $\langle L_n \rangle$  with bias is best organized when compared to the average shearing rate,  $\omega_s$  as is shown in Fig. 3. The shearing rate is normalized to the autocorrelation rate of  $I_{\text{sat}}$  fluctuations measured in the zero-shear state. An autocorrelation rate of  $\Delta\omega_d \approx 28\text{kHz}$  is calculated by taking the half-width at half-maximum of a Hilbert transform of the  $I_{\text{sat}}$  autocorrelation function. Confinement improvement (decreased  $\langle L_n \rangle$ ) occurs continuously and gradually with increasing  $\omega_s$  and reaches saturation for  $\omega_s \approx \Delta\omega_d$  (normalized  $\omega_s$  of 1). The confinement improvement appears to be largely independent of flow (or radial electric field) direction as IDD (filled points) and EDD (open points) flow cases follow the same trend when plotted against normalized shearing rate.

The change in confinement can be connected to a change in the fluctuation characteristics which dictate the turbulent flux. Fluctuation power in  $I_{\text{sat}}$  can be seen in the spectrum of Fig. 4. Most of the power is located in frequencies  $< 10\text{kHz}$  and in this range, power decreases overall with increasing shearing rate. A decrease of about one order of magnitude is seen between the lowest shearing point and the high shear regime. Above  $10\text{kHz}$ , power drops off considerably; however, just beyond  $\omega_s = \Delta\omega_s$ , a coherent mode emerges with a frequency

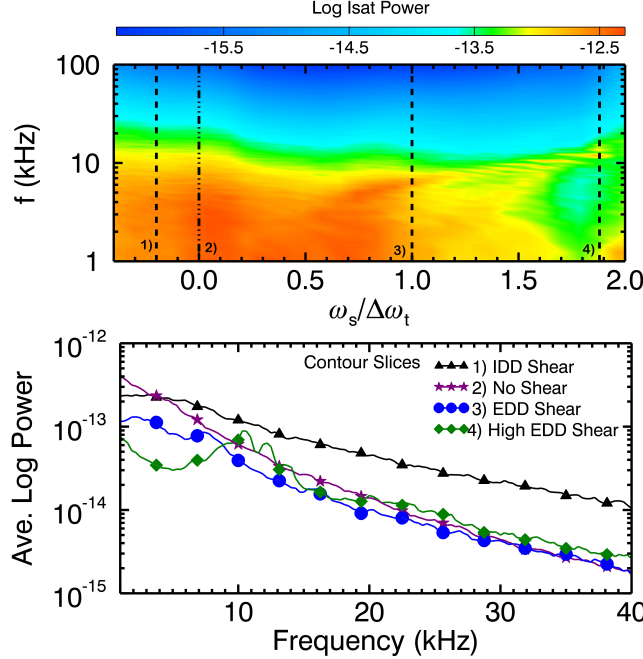


FIG. 4: Contour plot of  $\log I_{\text{sat}}$  fluctuation power versus shearing rate and frequency. Dashed lines show location of decorrelation rate. that begins at about 10kHz and increases linearly with shearing. The power at these high shearing rates is almost entirely located within this mode.

from  $I_{\text{sat}}$  radial profiles while particle flux,  $\Gamma_p = \langle \tilde{n} \tilde{v}_r \rangle = \langle \tilde{n} \tilde{E}_\theta \rangle / B$ , can be calculated spectrally as[22],

$$\Gamma_p = \frac{2}{B} \int_0^\infty |n(\omega)| |E_\theta(\omega)| \gamma_{n,E_\theta}(\omega) \cos[\phi_{n,E_\theta}(\omega)] d\omega \quad (1)$$

which allows for separate analysis of fluctuations, crossphase and coherency.

The changes in  $L_n$  and fluctuations are indicative of an overall change in particle flux. This flux can be directly measured by correlating  $I_{\text{sat}}$  with radial flow— $E \times B$  flow—using an  $E_\theta$  derived from two floating potential tips on either side of the  $I_{\text{sat}}$  measuring tip and rewritten in terms of the integral in (1). Like  $L_n$ , flux decreases with shearing rate as in Fig. 5; however, while flux decrease begin immediately with shearing, the decrease is not as fast as  $L_n$  with saturation not occurring until at least  $\omega_s > 2\Delta\omega_d$ . Flux decreases do not depend on flow direction either as again both IDD and EDD points fit on the same curve.

The calculated flux can be analyzed by its fluctuation and phase components separately as in Fig. 6. The top two plots show fluctuation power— $I_{\text{sat}}$  and azimuthal electric field ( $E_\theta$ )—as functions of normalized shearing rate, while the bottom two show crossphase and coherency between the two fluctuating quantities. As expected from the power contour plot,

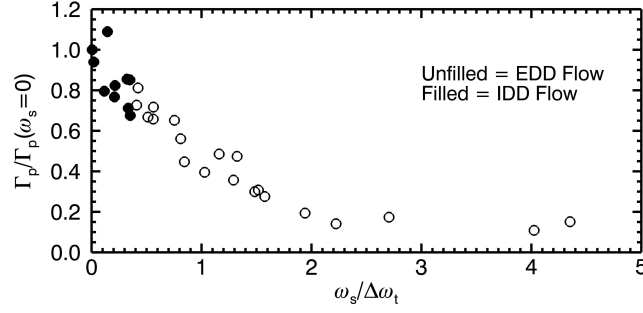


FIG. 5: Particle flux normalized to no-shear flux as a function of normalized shearing rate. Filled symbols represent points with flow in IDD.

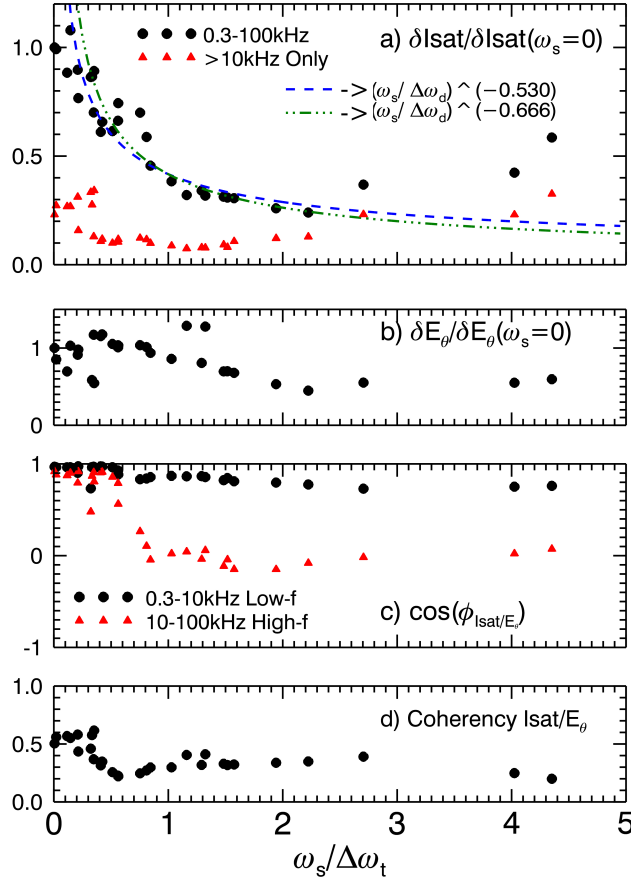


FIG. 6: Components of particle flux versus shearing rate including  $I_{sat}$ /Density fluctuation power(a), electric field fluctuation power(b), crossphase(c) and coherency(d) with black points for low frequency, red for high.

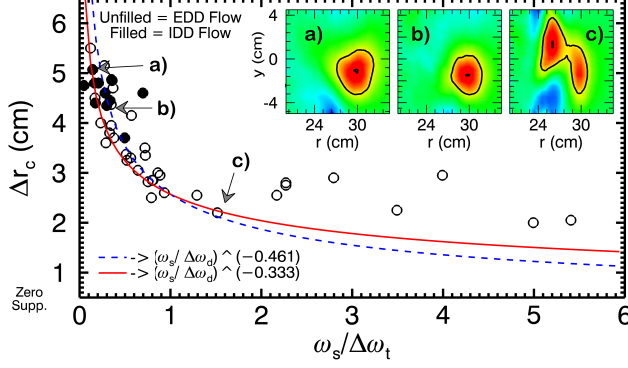


FIG. 7: Radially correlation lengths with reference probes at 28,29,30,31 or 32cm. Inset shows 2D correlation structure for IDD flow, no shear and high EDD flow. A mode pattern is seen at flow peak (26cm).

$I_{\text{sat}}$  fluctuations decrease with shearing for frequencies  $< 10\text{kHz}$ . Concurrently,  $\cos(\phi_{I_{\text{sat}}, E_\theta})$  for this bandwidth remains steady at nearly 1.0. Thus, since fluctuation power is concentrated in the low frequencies, overall flux is predominately suppressed by decreases in  $I_{\text{sat}}$  fluctuations, not crossphase. Note, however,  $I_{\text{sat}}$  fluctuations appear to increase beyond a normalized shearing of 2.0. These increases, however, are almost entirely from  $> 10\text{kHz}$  contributions suggesting that they originate from the coherent mode. Comparing to Fig. 5, it is clear these fluctuations do not contribute significantly to the flux. For high frequencies  $\cos(\phi_{I_{\text{sat}}, E_\theta})$  is nearly zero for  $\omega_s > \Delta\omega_d$ . Thus, despite increased fluctuations at high shear, no overall flux is observed.

As predicted by early theories on shear suppression, the effect of decreasing fluctuations is related to the shortening of a radial correlation length,  $\Delta r_c$ , for turbulent structures. Using a cross-correlation technique, we observe this modification of structures by azimuthal shearing as shown in Fig. 7.  $\Delta r_c$  is defined as the width of the contour plot at one-half its value at the reference point, represented by the black curve in the inset of Fig. 7. Like the flux and fluctuation data, the suppression begins with relatively little shearing and approaches a saturated value, though unlike flux, there appears to be a slight asymmetry in widths for IDD and EDD. This may be due to the influence of the coherent mode. In the high shearing regime shown in inset c) of Fig. 7, a mode pattern is observed in the peak EDD flow region and is distinct from the correlation structure. A similar, more diffuse mode may be present in the IDD flow region, but is more difficult to distinguish from the correlation structure thus adding to the apparent  $\Delta r_c$ .

Lastly, we can compare some of our results to theory. Considering the effect of shearing on eddy step size, the BDT model [17] predicts a power-law scaling of the form  $(\omega_s/\Delta\omega_t)^{-\alpha}$  for  $\tilde{n}$  and  $\Delta r_c$ . A comparison of the power fit to the predicted exponent is made for each quantity. As seen in Fig. 6 a best fit of  $\alpha = 0.530$  compares favorably to the BDT prediction of  $\alpha = 2/3$ . Similarly, a fit of  $\alpha = 0.461$  for  $\Delta r_c$  in Fig. 7 compares well to the BDT prediction of  $\alpha = 1/3$ . A cavaet: BDT theory is based on a constant density gradient while here gradients are always changing. Nevertheless, this initial agreement of data to model is promising for future comparisons.

This letter presents the first continuous variation shearing rate in a plasma device and has shown a clear effect of particle flux and density confinement through both the mechanisms of turbulent fluctuation and radial correlation length reduction.

---

- [1] K. Burrell, Phys. Plasmas **4**, 1499 (1997).
- [2] P. Terry, Rev. Mod. Phys. **72**, 109 (2000).
- [3] F. Wagner and et al., Phys. Rev. Lett. **49**, 1408 (1982).
- [4] R. Taylor, M. Brown, B. Fried, H. Grote, J. Liberati, G. Morales, P. Pribyl, D. Darrow, and M. Ono, Phys. Rev. Lett. **63**, 2365 (1989).
- [5] G. Tynan, L. Schmitz, R. Conn, R. Doerner, and R. Lehmer, Phys. Rev. Lett. **68**, 3032 (1992).
- [6] R. Weynants, G. V. Oost, G. Bertschinger, J. Boedo, P. Brys, T. Deligne, K. Dippel, F. Durodie, H. Euringer, K. Finken, et al., Nucl. Fusion **32**, 837 (1992).
- [7] J. Boedo, D. Gray, S. Jachmich, R. Conn, G. Terry, G. Tynan, G. V. Oost, R. Weynants, and T. Team, Nucl. Fusion **40**, 7 (2000).
- [8] C. Silva, H. Figueiredo, I. Nedzelskiy, B. Goncalves, and C. Varandas, Plas. Phys. Control Fusion **48**, 727 (2006).
- [9] D. Craig, A. Almagri, J. Anderson, J. Chapman, C. Chiang, N. Crocker, D. D. Hartog, G. Fiksel, S. Prager, J. Sarff, et al., Phys. Rev. Lett. **79**, 10 (1997).
- [10] B. Chapman, A. Almagri, J. Anderson, C.-S. Chiang, D. Craig, G. Fiksel, N. Lanier, S. Prager, J. Sarff, M. Stoneking, et al., Phys. Plasmas **5**, 1848 (1998).
- [11] M. Shats, K. Toi, K. Ohkuni, Y. Yoshimura, M. Osakabe, G. Matsunaga, M. Isobe, S. Nishimura, S. Okamura, K. Matsuoka, et al., Phys. Rev. Lett. **84**, 26 (2000).

- [12] O. Sakai, Y. Yasaka, and R. Itatani, Phys. Rev. Lett. **70**, 26 (1993).
- [13] J. Maggs, T. Carter, and R. Taylor, Phys. Plasmas **14**, 052507 (2007).
- [14] T. Carter and J. Maggs, Phys. Plasmas **16**, 012304 (2009).
- [15] P. Diamond, S.-I. Itoh, K. Itoh, and T. Hahm, Plasma Phys. Control Fusion **47**, R35 (2005).
- [16] G. Tynan, A. Fujisawa, and G. McKee, Plasma Phys. Control Fusion **51**, 113001 (2009).
- [17] H. Biglari, P. Diamond, and P. W. Terry, Phys. Fluids B. **2**, 1 (1990).
- [18] A. Ware, P. Terry, P. Diamond, and B. Carreras, Plasma Phys. Control Fusion **38**, 1343 (1996).
- [19] W. Amatucci, D. Walker, G. Ganguli, J. Antoniades, D. Duncan, J. Bowles, V. Gavriishchaka, and M. Koepke, Phys. Rev. Lett. **77**, 10 (1996).
- [20] W. Gekelman, H. Pfister, Z. Lucky, J. Bamber, D. Leneman, and J. Maggs, Rev. Sci. Instrum. **62**, 2875 (1991).
- [21] S. Zhou, W. Heidbrink, H. Boehmer, R. McWilliams, T. Carter, S. Vincena, B. Friedman, and D. Schaffner, Phys. Plasmas **19**, 012116 (2012).
- [22] E. Powers, Nucl. Fusion **14**, 749 (1974).